Dalton Transactions

Pyrazine-bridged Cu(II) chains: diaquabis(n-methyl-2-pyridone)copper(II) perchlorate complexes

Journal:	*Dalton Transactions*
Manuscript ID	DT-ART-08-2020-002716.R1
Article Type:	Paper
Date Submitted by the Author:	15-Sep-2020
Complete List of Authors:	Kirkman-Davis, Emma; Clark University, Department of Chemistry Witkos, Faith; Clark University, Department of Chemistry Selmani, Veli; Clark University, Department of Chemistry Monroe, Jeffrey; Clark University, Department of Chemistry Landee, Christopher; Clark University, Department of Physics Turnbull, Mark; Clark University, Department of Chemistry Dawe, Louise; Memorial University of Newfoundland, Chemistry; Wilfrid Laurier University Department of Chemistry and Biochemistry Polson, Matthew; University of Canterbury, Department of Chemistry Wikaira, Jan; University of Canterbury, Department of Chemistry

ARTICLE

Pyrazine-bridged Cu(II) chains: diaquabis(n-methyl-2-pyridone)copper(II) perchlorate complexes

Received 00th January 20xx,
Accepted 00th January 20xx

DOI: 10.1039/x0xx00000x

Emma Kirkman-Davis,[a] Faith E. Witkos,[a] Veli Selmani,[a] Jeffrey C. Monroe,[a] Christopher P. Landee,[b] Mark M. Turnbull,[a,*] Louise N. Dawe,[c] Matthew Polson[d] and Jan L. Wikaira[d]

A family of pyrazine-bridged, linear chain complexes of Cu(II) of the formula $[CuL_2(H_2O)_2(pz)](ClO_4)_2$ [pz = pyrazine; L = n-methyl-2(1H)-pyridone, n = 3 (**1**), 5 (**2**), and 6 (**3**)] has been prepared. Single-crystal X-ray diffraction shows six-coordinate, pyrazine-bridged chains with trans-pairs of ancillary ligands. The substituted pyridine molecules exist in their pyridone tautomers and are coordinated through the carbonyl oxygen atom. The structure is stabilized by intramolecular hydrogen bonds between the pyridone and water molecule, and via hydrogen bonds between the water molecules and perchlorate ions. **2** undergoes a crystallographic phase transition between *C*2/c (high temperature phase) and *P*-1 (low temperature phase). Powder EPR spectra reveal that all complexes are rhombic, although differences between g_x and g_y can only be seen clearly at Q-band. Variable temperature magnetic susceptibility data show antiferromagnetic interactions and the data were fit to the uniform chain model yielding J/k_B = -9.8, -9.2 and -11 K for **1**-**3** respectively. Attempts to model an interchain interaction strength indicate that the chains are very well isolated.

Introduction

Understanding of the physical parameters controlling magnetic exchange in the solid state has been of interest to chemists and physicists for decades[1] and interest continues to the present.[2] Studies of magnetostructural correlations may be simplified by examining low-dimensional lattices; that is, lattices where the magnetic exchange interactions occur in fewer than three dimensions. This includes layers, ladders, chains and zero-dimensional systems such as dimers and clusters. The uniform magnetic chain (a one-dimensional lattice) has been of great interest and the interpretation of the magnetic properties of such systems became routine with the pioneering work of Bonner and Fisher on the development of models for those materials.[3] One of the most well-studied 1D-families are the pyrazine-bridged Cu(II) complexes, as exemplified by $Cu(pz)(NO_3)_2$ [pz = pyrazine].[4] The magnetic properties and degree of isolation of the complex have been studied by multiple techniques including variable temperature and field magnetization ,[5] EPR,[6] infrared spectroscopy,[7] density functional analysis,[8] NMR,[9] μSR,[10] neutron spectroscopy,[11] thermal expansion effects,[12] and electron density analysis[13] among other techniques[14] making it, perhaps, the most thoroughly studied 1D-system.

Pyrazine is used almost ubiquitously as a bridging ligand in coordination chemistry both because it provides a dicoordinating bridge that is rigorously linear and because it is a good bridge for antiferromagnetic superexchange, especially for compounds of the azaphilic Cu(II) ion. In addition to the linear chain-type compounds described above, pyrazine and its derivatives have been employed in the formation of ladder structures[15] and layer compounds, both square[16] and rectangular.[17] Similar structures incorporating other metal ions with a wide range of interesting magnetic, conductivity and optical properties have also been prepared and studied including one-[18] and two-dimensional pyrazine bridged systems.[19] However, although always antiferromagnetic, the magnitude of the exchange propagated through pyrazine itself ranges widely, typically -5 to -18 K (J/k_B), in Cu(II) compounds alone[20] while the layered compound $Ni(pz)_2(ClO_4)_2$ exhibits virtually no magnetic exchange.[21]

We became interested in the parameters controlling the strength of the exchange through the pyrazine bridge and were interested in developing a family of isostructural compounds where changes to the Cu-pz-Cu linkage were minimized and the effect of ancillary ligands on the electron density at the Cu(II) ion could be considered. The synthesis and structure of $[Cu(5\text{-chloro-2(1H)-pyridone})_2(H_2O)_2(pz)](ClO_4)_2$ (Fig. 1) by Ng *et al.*[22] inspired our selection of a family for study. The chlorine substituents of the 2(1*H*)-pyridone molecule are distant from the copper pyrazine chains, but may still reduce electron density in the pyridone ring and thus change its donating properties with respect to the copper ion. This suggested that a family of compounds could be made by varying the position of the substituent (3,4,5,6) and its electron donating/withdrawing nature without significant structural changes to the chain. Here we report the synthesis, structure and magnetic properties (via EPR and variable temperature magnetic susceptibility measurements) of the methyl-substituted compounds $[Cu(L)_2(H_2O)_2(pz)](ClO_4)2$ [L = n-Me-2(1H)-pyridone, where n = 3 (**1**), 5 (**2**), and 6 (**3**)].

[a] Carlson School of Chemistry and Biochemistry and the
[b] Department of Physics, Clark University, 950 Main Street, Worcester, MA 01610.
[c] Department of Chemistry and Biochemistry, Wilfrid Laurier University, 75 University Avenue West, Waterloo, Ontario N2L 3C5.
[d] Department of Physical and Chemical Sciences, University of Canterbury, Private Bag 4800, Christchurch, New Zealand.

Electronic Supplementary Information (ESI) available: [details of any supplementary information available should be included here]. See DOI: 10.1039/x0xx00000x

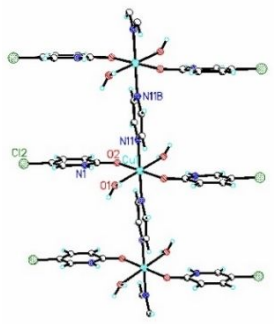

Figure 1. The structure of [Cu(5-chloro-2(1H)-pyridone)$_2$-(H_2O)$_2$(pz)](ClO_4)$_2$ from Ref. 20 (perchlorate ions not shown).

Experimental

Materials and methods

3-Methyl-2-pyridone and 5-methyl-2-pyridone were purchased from Ark Pharmaceuticals while 6-methyl-2-pyridone was purchased from Matrix Scientific. Copper(II) perchlorate hexahydrate and pyrazine (pz) were purchased from Sigma-Aldrich. All materials were used as received. Note: perchlorates are potentially explosive and should be used and prepared in small quantities. "50% methanol" refers to a 50:50 solution of methanol and water by volume. FTIR spectra were recorded on a Perkin-Elmer Spectrum 100 spectrometer via ATR. X-Ray powder diffraction data were collected with a Bruker AXS-D8 X-ray Powder Diffractometer. Elemental analyses were performed at the Marine Science Institute, University of California Santa Barbara, CA.

Synthetic procedures

Catena-[Cu(3-methyl-2-pyridone)$_2$(H_2O)$_2$(μ-pz)](ClO_4)$_2$ **1**

Pyrazine (0.083 g, 1.0 mmol) was added to 3-methyl-2-pyridone (0.226g, 2.0 mmol) and dissolved in 3.0mL of 50% methanol to give a colorless solution. Copper(II) perchlorate hexahydrate (0.369g, 1.0 mmol) was dissolved in 5.0mL of 50% methanol (blue). The solutions were combined which formed a green solution. After six days of slow evaporation, dark green crystals had formed on the bottom of the beaker. The crystals were isolated by vacuum filtration, rinsed quickly with cold distilled water and left to dry. Yield: 0.401 g, 67%. CHN calcd (exp): C 32.20 (32.19), H 3.94 (3.72), N 9.32 (9.39). IR (cm^{-1}) 3558 (w), 3417 (w), 1631 (m), 1562 (w), 1513 (m), 1563 (m), 1412 (m), 1386 (m), 1271 (w), 1104 (s), 1073 (s), 826 (m), 778 (s), 620 (m).

Catena-[Cu(5-methyl-2-pyridone)$_2$(H_2O)$_2$(pz)](ClO_4)$_2$ **2**

Pyrazine (0.093 g, 1.1 mmol) was added to 5-methyl-2-pyridone (0.227 g, 2.0 mmol) in 3.5mL of 50% methanol to generate a colorless solution. Copper(II) perchlorate hexahydrate (0.386g, 1.0 mmol) was dissolved in 3.5mL of 50% methanol (blue). The organic solution was added to the copper perchlorate hexahydrate solution yielding a green solution. After five days of slow evaporation, long rod-shaped green crystals had formed. The crystals were isolated by vacuum filtration, rinsed quickly with cold distilled water, and left to dry. Yield: 0.317 g, 53%. CHN calcd (exp): C 32.20 (33.10), H 3.72 (3.84), N 9.39 (9.46). IR (cm^{-1}) 3440 (br, w), 3278 (w), 3176 (w), 1655 (m), 1603 (s), 1550 (m), 1420 (w), 1408 (m), 1381 (w), 1150 9m), 1112 (s), 1043 (s), 920 (m), 829 (s), 769 (m), 621 (s).

Catena-[Cu(6-methyl-2-pyridone)$_2$(H_2O)$_2$(pz)](ClO_4)$_2$ **3**

Pyrazine (0.082 g, 1.0 mmol) was added to 6-methyl-2-pyridone (0.222g, 2.0 mmol) in 4.0mL of 50% methanol (pale yellow). Copper(II) perchlorate hexahydrate (0.402g, 1.0 mmol) was dissolved in 4.0mL of 50% methanol (blue). The solutions were combined to form a green solution. After one week of slow evaporation, large green crystals had formed on the sides of the beaker. The crystals were isolated by vacuum filtration, rinsed quickly with cold distilled water, and left to dry. Yield: 0.395 g, 66%. CHN calcd(exp): C 32.22 (32.20), H 3.81 (3.72), N 9.34 (9.39). IR (cm^{-1}) 3417 (w), 2967 (w), 1642 (m), 1627 (m), 1421 (m), 1397 (m), 1270 (w), 1169 (m), 1076 (s), 1002 (m), 801 (m), 726 (m), 621 (m), 586 (m).

Crystallography

Data collections were carried out on a Bruker Apex-II CCD diffractometer with Cu Kα λ=1.5418 Å (**2**, **1** and **3** high temperature) or Mo Kα λ = 0.71073 Å (**1, 3**, low temperature) radiation and a graphite monochromator. The structures were solved by direct methods, SHELXS-97[23] or SHELXT,[24] and refined using least-squares analysis via SHELXL-2016.[25] Non-hydrogen atoms were refined anisotropically. Hydrogen atoms bonded to carbon atoms were placed in calculated positions and refined via a riding model using fixed isotropic thermal parameters. Other hydrogen atoms were located in the difference Fourier maps, with fixed isotropic thermal parameters used for position refinement. Compound **2** undergoes a temperature dependent phase transition from monoclinic, C2/c (designated **2**HT) to triclinic, P-1 (designated **2**LT) near 170 K with twinning and fracturing of the crystal. The low temperature structure was solved and refined using only the major multi-crystal component. Cell constants, refinement parameters, etc. are provided in Table 1. Selected bond lengths and angles are given in Table 2. Table 3 contains hydrogen bonding data. Calculated powder patterns from crystallographic data of **1-3** were compared to powder X-ray diffraction data to verify the phase and purity of the bulk samples used for magnetic data collection (see SI - Figs S10-12). Initial weak comparison of the calculated spectrum for **1** and the experimental data led to a new data collection 280 K. No phase transition was observed, but the room temperature unit cell provided an excellent match to the powder data. Data were also collected for **3** at 280 K and no phase transition was observed. Data have been deposited with the CCDC as deposit numbers: 2017465 (**1**, 280 K), 2017463 (**1**, 153 K), 2017466 (**2**, 220 K), 2017467 (**2**, 120 K), 2018693 (**3**, 280 K), 2017464 (**3**, 153 K).

Magnetic data collection

Magnetic susceptibility data were collected via a Quantum Design MPMS-XL SQUID magnetometer. Powdered samples of **1-3** were packed into gelatin capsules and fit into drinking straws attached to sample rods. Magnetization of samples at 1.8K was measured in increasing field from 0 to 50 kOe, and selected values as the field decreased to zero, which showed no hysteresis. Temperature dependent susceptibility data were collected in 1 kOe from 1.8 to 310 K. Background corrections were made for the signal of the gelatin capsule and straw (measured independently), the

temperature independent paramagnetism of the copper(II) ion and the diamagnetism of the constituent atoms, estimated via Pascal's constants.[26] Data were fit to the Hamiltonian $\boldsymbol{H} = -\boldsymbol{J}\sum \boldsymbol{S_1}\bullet\boldsymbol{S_2}$.

EPR

Powder EPR spectra were collected on a Bruker EMX EPR spectrometer operating at X-band (9.7 GHz) and Q-band (34 GHz) frequencies with 100 kHz field modulation. The field was calibrated with DPPH prior to data collection at X-band and while data processing at Q-band. All spectra were fit using EasySpin[27] in MATLAB.[28] Crystals of each compound were ground to an extremely fine powder with a mortar and pestle for the polycrystalline EPR data collection. For data collection at Q-band, samples were packed in borosilicate glass capillary tubes.

Table 1. X-ray data collection and refinement parameters for **1-3**.

Compound	**1**	**2**(HT)	**2**(LT)	**3**
Formula	$C_{16}H_{22}Cl_2CuN_4O_{12}$	$C_{16}H_{22}Cl_2CuN_4O_{12}$	$C_{16}H_{22}Cl_2CuN_4O_{12}$	$C_{16}H_{22}Cl_2CuN_4O_{12}$
Mol. Wt.	596.81	596.81	596.81	596.81
Temp (K)	153(2)	220(2)	120(2)	153(2)
Crystal System	Triclinic	Monoclinic	Triclinic	Monoclinic
Space Group	$P\bar{1}$	*C*2/c	$P\bar{1}$	*C*2/m
Unit cell: a(Å)	6.848(3)	15.0161(2)	6.8463(3)	23.016(11)
b(Å)	8.153(3)	6.86470(10)	8.0507(5)	6.822(3)
c(Å)	10.334(4)	22.3242(3)	11.6595(6)	7.656(4)
α (°)	90.510(7)	90	79.958(5)	90
β (°)	98.788(12)	93.3680(10)	73.894(4)	90.189(8)
γ (°)	94.272(9)	90	66.235(5)	90
Volume (Å)	568.5(4)	2297.23(5)	563.63(6)	1202.1(10)
Z	1	4	1	2
Abs. Coef (mm^{-1})	1.267	4.134	4.212	1.198
Crys. Dim. (mm)	0.30x0.07x0.06	0.72x0.43x0.18	0.72x0.43x0.18	0.49x0.45x0.41
θ/2θ range (°)	2.51-30.91	5.90-73.25	6.02-73.50	3.11-30.21
Index ranges	-9 ≤ h ≤ 9 -11 ≤ k ≤ 10 -12 ≤ l ≤ 13	-18 ≤ h ≤ 18 -8 ≤ k ≤ 8 -27 ≤ l ≤ 27	-8 ≤ h ≤ 8 -9 ≤ k ≤ 9 -14 ≤ l ≤ 14	-30 ≤ h ≤ 30 -8 ≤ k ≤ 9 -10 ≤ l ≤ 8
Total Rlfn	6336	21728	10701	6233
Completeness	0.840	0.995	0.976	0.873
Ind. Rlfn (R_{int})	3007 (0.0203)	2305 (0.0375)	2213 (0.0361)	1686 (0.0293)
Min-max. trans.	0.7405-0.9564	0.4351-1.000	0.5077-1.000	0.6187-0.7581
Data/restr./param.	3007/1/218	2305/2/171	2213/2/170	1686/0/106
GooF	1.042	1.122	1.254	1.122
Fin. $R_1(wR_2)I>2\sigma$	0.0348 (0.0866)	0.0283 (0.0741)	0.0579 (0.1660)	0.0380 (0.1074)
Fin. $R_1(wR_2)$ all	0.0359 (0.0876)	0.0293 (0.0749)	0.0583 (0.1663)	0.0382 (0.1076)
Peak(hole) ($e/Å^3$)	0.407 (-0.564)	0.334 (-0.327)	2.583 near N1 (-0.651)	0.642 (-0.594)

Table 2. Bond lengths (Å) and angles (°) of **1-3**.

Compound	**1** (153 K)	**2**(HT)	**2**(LT)	**3**
Cu1-N1	2.0362(15)	2.047(2)	2.033(3)	2.023(2)
Cu1-N4		2.043(2)		
Cu1-O12	1.9556(13)	1.9475(12)	1.946(3)	1.954(2)
Cu1-O1W	2.454(2)	2.3868(13)	2.385(3)	2.470(2)
O12-C12	1.280(2)	1.278(2)	1.275(5)	1.274(3)
O12-Cu1-O12a	180	179.53(7)	180	180
O1W-Cu-O1Wa	180	177.08(6)	180	180
N1-Cu1-N1	180		180	180
N1-Cu1-N4b		180		
N1-Cu1-O12	90.01(5)	90.24(3)	89.35(12)	90
N4b-Cu1-O12		89.76(3)		
N1-Cu1-O1W	89.10(5)	88.54(3)	89.75(11)	90
O12-Cu1-O1W	85.70(5)	84.47(5)	83.49(10)	84.90(9)

Cu1-O12-C12	134.90(11)	134.59(11)	133.6(2)	135.71(17)
Symm. Op. a = 1-x, y, 0.5-z; b = x, y+1, z.				

Results and Discussion

Synthesis

The reaction of $Cu(ClO_4)_2 \cdot 6H_2O$, with two equivalents of the appropriate n-methyl-2(1H)-pyridone (n-Me-2-pyone) in methanol/water yielded three compounds: $[Cu(n\text{-}Me\text{-}2\text{-}pyone)_2(H_2O)_2(pz)](ClO_4)_2$ (n = 3, **1**; n = 5, **2**; n = 6, **3**) in 50-70% yield (Figure 2). Green crystals suitable for single crystal X-ray diffraction were obtained upon slow evaporation at room temperature. All compounds form pyrazine bridged chains with two coordinated 2-pyone molecules and two coordinated water molecules. Perchlorate ions are located between the chains and their positions are stabilized by hydrogen bonding. Despite repeated attempts under a variety of conditions in various solvents and solvent mixtures, we were unable to isolate the corresponding 4-methyl-2-pyridone compound.

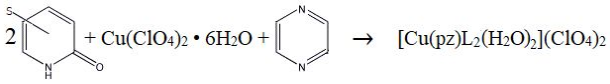

Figure 2. Preparation of compounds **1-3** in 50% methanol.

Crystal Structures

Compound **1** crystallizes in the triclinic space group P-1 with one formula unit in the unit cell. Selected bond lengths and angles are given in Table 2 and the local coordination sphere is shown in Figure 3. The copper ion is coordinated to two 3-Me-2-pyone molecules, two water molecules and a bridging pyrazine molecule, generating pseudo-octahedral local symmetry. A classic Jahn-Teller (J-T) distortion is observed with significant elongation of the Cu-water axis [Cu-O1W = 2.453(2)]. The Cu-N1 and Cu-O12 bonds occupy the equatorial plane and the bond lengths are typical. The Cu(II) ion is located on an inversion center, rendering all trans-bond angles 180°. O12, O12a, N1 and N1A form the equatorial plane (planar as required by symmetry) and the Cu1-O1W bond is 4.4° from the normal to that plane. The pyrazine ring is planar (as required by symmetry) and is canted 30.2° relative to the equatorial plane. The pyridone ring is nearly planar (mean deviation of constituent atoms = 0.0077Å) and is significantly canted relative to the equatorial plane (75.2°). The perchlorate ion is two-site disordered with refined occupancies of 0.677 (Cl1) and 0.323 (Cl'). A figure showing the two sites is presented in the SI (Figure S1a). A room temperature data collection reveals the same unit cell, space group and disordered perchlorate ion (see SI for data collection and cell parameters).

The bridging pyrazine molecule creates chains parallel to the *a*-axis (see Figure 4). The pyridone molecules of adjacent chains are interdigitated relative to the *c*-axis to minimize the void volume between those chains. The shortest interchain Cu…Cu distance parallel to the *c*-axis is just over 10.3 Å, while the shortest interchain Cu…Cu distance parallel to the *b*-axis is just greater than 8.1 Å.

Figure 3. The molecular unit of **1** showing 50% probability thermal ellipsoids. Hydrogen atoms are shown as spheres of arbitrary size. Only the asymmetric unit, Cu coordination sphere and those hydrogen atoms whose positions were refined are labelled. Only

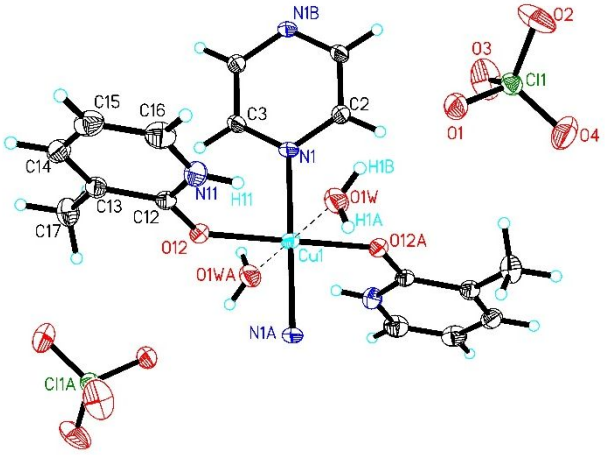

one position for the disordered perchlorate ion is shown for clarity. Symmetry equivalent atoms 'A' are related by the inversion center at Cu1. Those labelled B are related by the inversion center in the middle of the pyrazine ring.

Figure 4. A packing diagram of **1** viewed parallel to the *b*-axis showing the chain formation and offset of adjacent chains along the *c*-axis. Dashed lines represent hydrogen bonds.

Intramolecular hydrogen bonds are observed between the N-H of

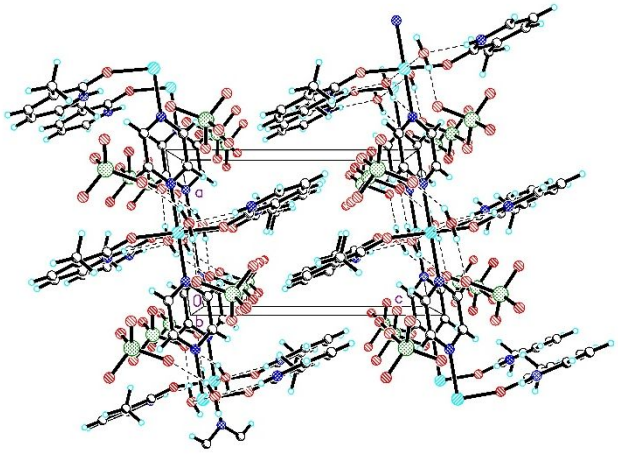

the pyridone ligands and the coordinated water molecules (see Table 3 for parameters). The water molecules also act as hydrogen bond donors to the perchlorate ions, helping to stabilize their position in the lattice where those ions serve to separate the chains parallel to the *b*-axis (see Figure 5).

Table 3. Hydrogen bonding parameters for **1**-**3**.

Cmpd/bond	D-H (Å)	H…A (Å)	D…A (Å)	D-H …A(°)
1				
N11-H11…O1W	0.83(3)	2.00(3)	2.807(2)	165(2)
O1W-H1A…O1	0.78(2)	1.99(2)	2.762(3)	175(3)
O1W-H1B…O1a	0.78(2)	2.21(2)	2.957(3)	158(3)
2(HT)				
N11-H11…O1W	0.77(3)	2.15(3)	2.831(2)	148(3)
O1W-H1A…O1	0.809(16)	2.020(17)	2.818(2)	169(2)
O1W-H1B…O1a	0.805(17)	2.116(18)	2.904(2)	166(2)
2(LT)				
N11-H11…O1W	0.92(6)	2.02(6)	2.823(5)	145(4)
O1W-H1A…O2	0.84(2)	2.00(3)	2.799(4)	158(5)
O1W-H1B…O1	0.83(2)	2.04(2)	2.873(4)	176(5)
3				
N11-H11…O1W	0.89(4)	1.91(4)	2.782(3)	168(4)
O1W-H1A…O2	0.78(3)	1.98(3)	2.755(3)	170(3)

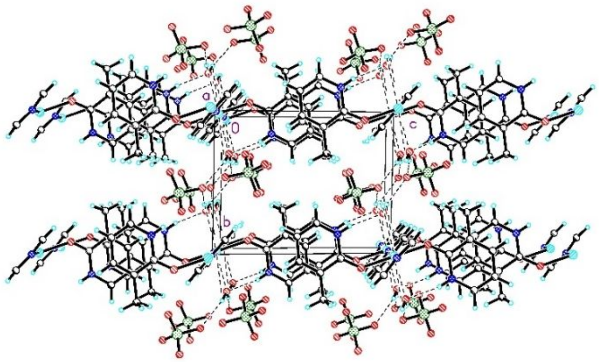

Figure 5. A packing diagram of **1** viewed parallel to the *a*-axis (parallel to the chains) showing the isolation of the chains. The perchlorate ions are located between the chains along the *b*-axis generating an alternating layer-type structure. Dashed lines represent hydrogen bonds.

Compound **2** (5-methyl-2-pyone) undergoes a crystallographic phase transition as a function of temperature. At high temperature (**2**HT), the structure is monoclinic, *C*2/*c* while at low temperature the structure (**2**LT) is triclinic, *P*-1. Initial comparison of the RT powder data to the structure at 120 K showed a significant mismatch, prompting a variable temperature study. Crystallographic data were collected at five temperatures from 220 K to 120 K. The high and low temperature data are summarized in Tables 1-3. Full details of the temperature dependence of the cell parameters are given in the Supp. Inf. (Table S1). The compound undergoes a color change in conjunction with the phase transition (see Figure 6).

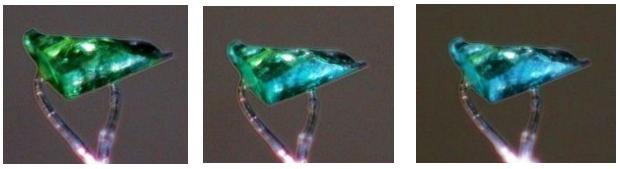

Figure 6. The color of **2** as a function of temperature.

The molecular unit of **2**HT is shown in Figure 7. It resembles the structure of **1** with some significant differences. The Cu1 ions sits on a two-fold axis, rather than an inversion center and as such there are two unique Cu-N bonds to the pyrazine ring which are both slightly longer (~ 0.01 Å) than observed in **1**. The Cu1-O1W bond (along the J-T axis) is significantly shorter (~0.07 Å) and the Cu1-O12 bond is slightly shorter (~ 0.01 Å) giving a slightly more compressed coordination sphere. The equatorial plane is still formed by the coordinated pyrazine and pyridone molecules, with the Cu1-O1W bond inclined 5.7° from the normal to that plane. The pyrazine ring is canted 35.6° from the equatorial plane while the pyridone ring is significantly more canted (86.3°) and nearly perpendicular to the equatorial plane.

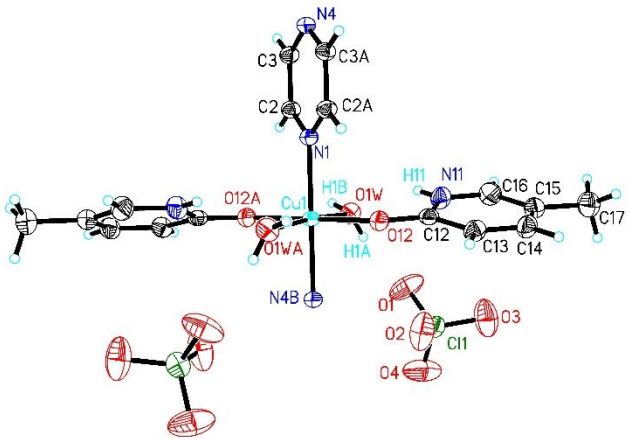

Figure 7. The molecular unit of **2**(HT) showing 50% probability thermal ellipsoids. Hydrogen atoms are shown as spheres of arbitrary size. Only the asymmetric unit, Cu coordination sphere and those hydrogen atoms whose positions were refined are labelled. Symmetry equivalent atoms 'A' are related by the 2-fold rotation axis at Cu1. Those labelled B are related by a unit cell translation parallel to the *b*-axis.

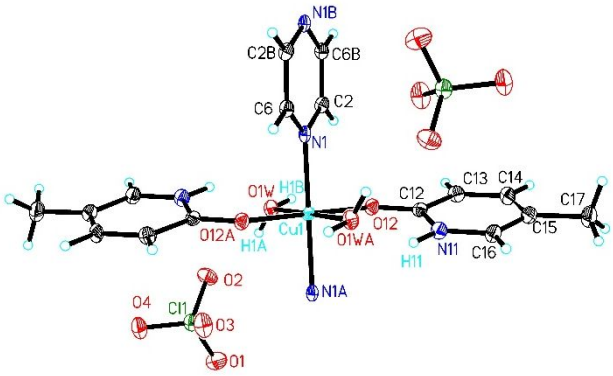

Figure 8. The molecular unit of **2**(LT) showing 50% probability thermal ellipsoids. Hydrogen atoms are shown as spheres of arbitrary size. Only the asymmetric unit, Cu coordination sphere and those hydrogen atoms whose positions were refined are labelled. Symmetry equivalent atoms 'A' are related by the inversion center at Cu1. Those labelled B are related by the inversion center in the middle of the pyrazine ring.

The molecular unit of **2**(LT) is shown in Figure 8. While similar in appearance to that of the high temperature version, there are some notable differences from the reduction in symmetry to *P*-1. The copper(II) - oxygen bonds are nearly identical in length despite the temperature and phase changes, but the Cu1-N1 bond has shortened by just over 0.01 Å. Because the Cu1 ion sits on a crystallographic inversion center, all trans bonds are 180° as required by symmetry and the Cu1-O1W bond is slightly more inclined relative to the equatorial plane (6.5°). The canting of the pyrazine ring to the equatorial plane is comparable (36°), but the canting of the pyridone ring (75.1°) more closely resembles **1** than **2**(HT). An overlay of the molecular units of **2**(LT) and **2**(HT) is shown in Figure S4.

The change in position of the methyl group on the pyridone ring results in a greater offset between chains parallel to the *c*-axis compared to **1** for both phases [11.6 Å, **2**(HT); 11.7 Å, **2** (LT)], but different responses along the *a*- axis where the separation is significantly longer for **2**(HT) (8.25 Å) than for **2**(LT) (8.05 Å). Figure 9 shows the packing of **2**(HT); Figure S3 shows the comparable view for **2**(LT).

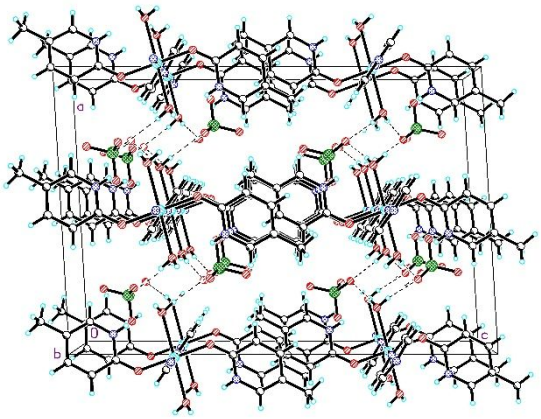

Figure 9. A packing diagram of **2** (HT) viewed parallel to the *b*-axis (parallel to the chains) showing the isolation of the chains. The perchlorate ions are located between the chains along the *a*-axis generating an alternating layer-type structure. Dashed lines represent hydrogen bond donors.

Compound **3** crystallizes in the monoclinic space group *C*2/*m*. The Cu1 ion sits on both the 2-fold axis and a mirror plane. The molecular unit is shown in Figure 10. The combination of symmetry elements requires only one unique C-atom (C2) for the pyrazine ring. Similarly, the pyridone rings and the CuO_4 plane are exactly planar (they lie on a mirror) and the Cu-N1 bond is perpendicular to that plane as required by symmetry. The coordinated water molecules occupy the J-T axis and lie 5.1° away from the normal to the equatorial plane. There are three symmetry unique oxygen atoms on the perchlorate ion, one of which is slightly disordered across the mirror plane (Figure S1b).

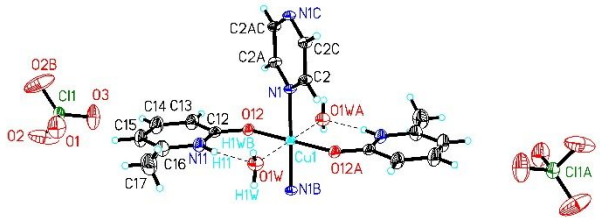

Figure 10. The molecular unit of **3** showing 50% probability thermal ellipsoids. Hydrogen atoms are shown as spheres of arbitrary size. The asymmetric unit, Cu coordination sphere and those hydrogen atoms whose positions were refined are labelled. Symmetry equivalent atoms A are related by the 2-fold axis passing through Cu1. Those labelled B are related by the mirror plane at y = 0. Those labelled C are related by the mirror plane at y = 0.5. Only one position of the disordered perchlorate ion is shown.

EPR

X-band: The powder EPR spectra of **1**-**3** were collected at X-band frequency (9.4 GHz) at room temperature; the experimental and fitted spectra are shown in Figures 11-13. It is not immediately obvious if the spectra are axial or rhombic, particularly so for the spectrum of **3**, although the coordination environment in all three 6-coordinate 2+2+2 complexes suggest rhombic electronic structure (where gx = gy ≠ gz is axial and gx ≠ gy ≠ gz is rhombic).

EasySpin[27] was used to fit the spectra and the resulting fit parameters are tabulated in Table 4, according to the Zeeaman interaction $\boldsymbol{E = g\mu_b B}$, where *g* is the anisotropic g-tensor, $\boldsymbol{\mu_b}$ is the Bohr magneton and *B* is the magnetic field. The fit to each spectrum allowed the g-tensor to refine anisotropically giving g_x, g_y, and g_z. The linewidth parameters were modeled using an approximate linear combination of the Gaussian and Lorentzian contributions to the lineshape. The g-strain parameter was used to account for inhomogeneous Gaussian broadening of the line. The fits to **1**-**3** exhibited three distinct g-factors, agreeing with the expected rhombic electronic structure (Table 4). The lineshape was found to be dominated by the Lorentzian contribution.

The contribution from g-strain on g_x and g_y were negligible for all g-factor values across the three spectra. The only significant g-strain contribution was for g_z, which agrees with the expectation that g-strain is proportional to g. This is because the molecular z-axis has the largest local distribution of coordination environment causing greater inhomogeneous broadening.

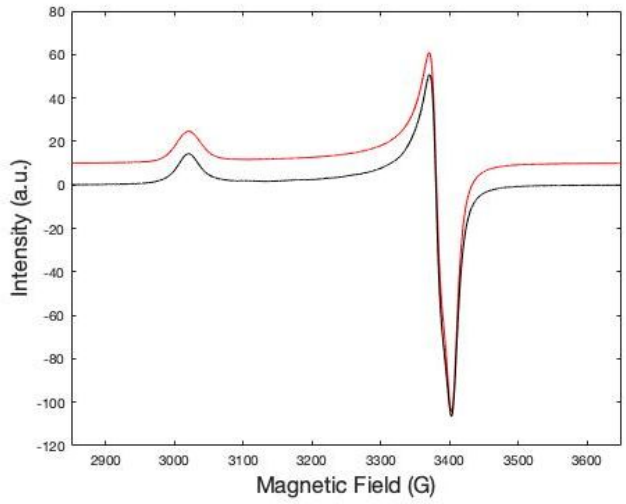

Figure 11. Powder EPR spectrum of **1** collected at room temperature and X-band frequency. Data are shown in black while the fit to the data is shown in red.

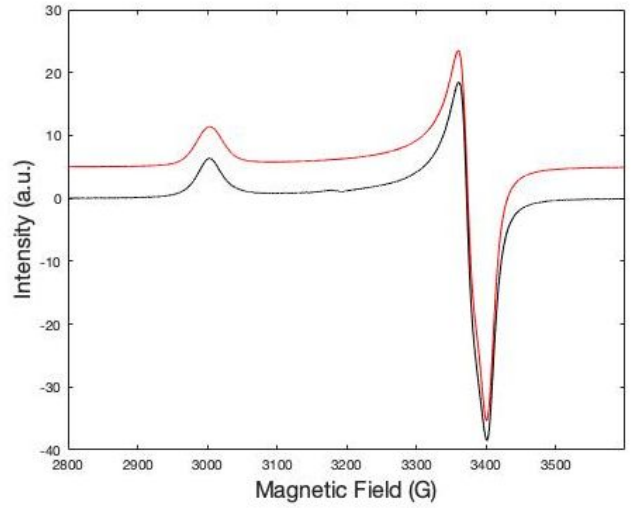

Figure 12. Powder EPR spectrum of **2** collected at room temperature and X-band frequency. Data are shown in black while the fit to the data is shown in red. The small anomaly near 3200 G may indicate the presence of a slight impurity; it was neglected in fitting the data.

Table 4. Parameters of fitted EPR spectra of **1**-**3** collected at X-band (X) and Q-band (Q) frequencies.

	1 (X)	**1** (Q)	**2** (X)	**2** (Q)	**3** (X)	**3** (Q)
g_x	2.0561	2.0509	2.0577	2.0511	2.0577	2.0523
g_y	2.0705	2.0661	2.0759	2.0708	2.0677	2.0624
g_z	2.3174	2.3095	2.3316	2.3231	2.3148	2.3060
g_{strain} ($x10^{-2}$)	2.43		2.49		2.49	
g_{ave}	2.1480	2.1422	2.1551	2.1483	2.1467	2.1402
GC	0.6847	0.6103	1.0573	0.8462	0.5527	0.5004
LC	1.7545	1.7149	1.9962	1.9255	1.7793	2.6364
RMSD	0.0058	0.0119	0.0057	0.0128	0.0032	0.0111

GC = Gaussian contribution; LC = Lorentzian contribution.

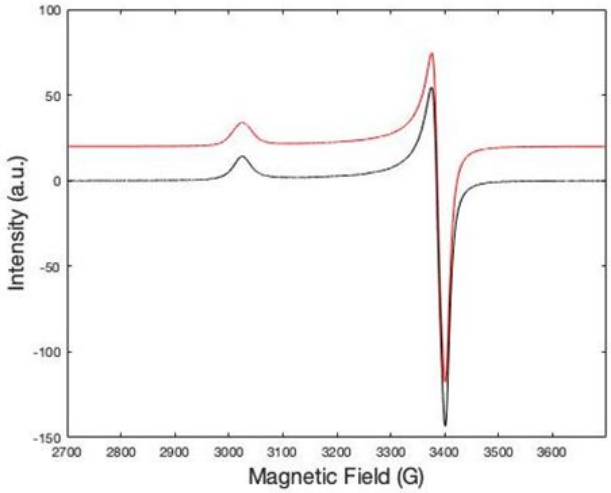

Figure 13. Powder EPR spectrum of **3** collected at room temperature and X-band frequency. Data are shown in black while the fit to the data is shown in red.

Q-band: To increase the resolution of the above spectra for **1**-**3**, powder EPR data were collected at Q-band frequency (34 GHz) at room temperature. The experimental and fitted spectra are shown in Figures 14-16. EasySpin[27] was used to fit the spectra and the resulting fit parameters are tabulated in Table 4. The fitted parameters were as described in the X-band experimental analysis. The g-strain contributions were found to be negligible for all g-factors. Note that the spectrum in Figure 14 is not smooth between g_z and g_y, which could be a result of orientation dependence in the polycrystalline sample that was not detectable at X-band frequency. Regardless, the extremum features are clear and the RMSD is satisfactory (Table 4).

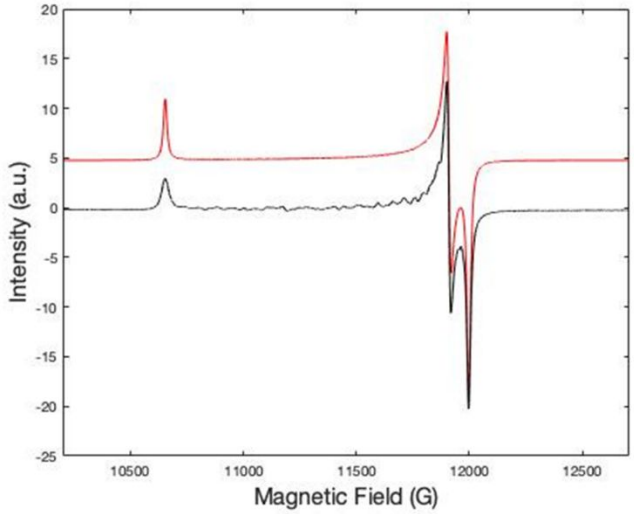

Figure 14. Powder EPR spectrum of **1** collected at room temperature and Q-band frequency. Data are shown in black while the fit to the data is shown in red.

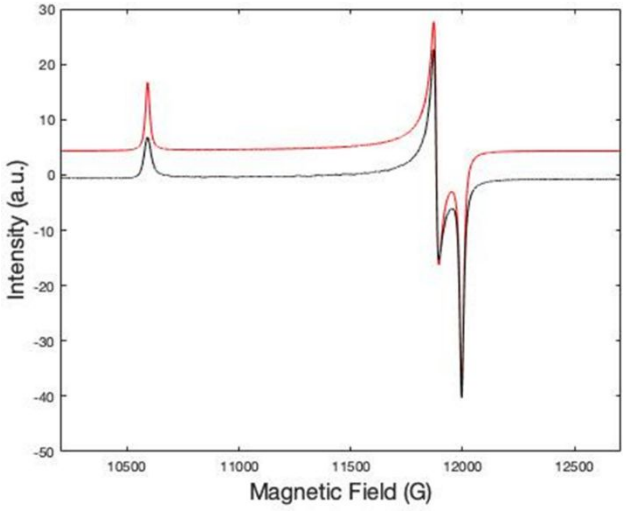

Figure 15. Powder EPR spectrum of **2** collected at room temperature and Q-band frequency. Data are shown in black while the fit to the data is shown in red.

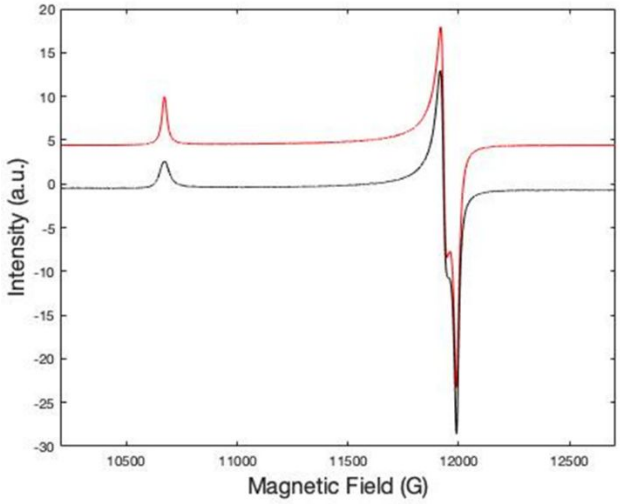

Figure 16. Powder EPR spectrum of **3** collected at room temperature and Q-band frequency. Data are shown in black while the fit to the data is shown in red.

There are some key differences were noted between the X-band and Q-band spectra. The fitted values of the g-factor, the Gaussian contribution to the linewidth, and the Lorentzian contribution to the linewidth are all consistently larger for fits at X-band than for fits at Q-band, with the exception of the Lorentzian contribution of **3**; the RMSD values are consistently smaller (Table 5). Compound **3** has the only EPR spectrum at Q-band in which the g_y and g_x resonances are not well-resolved, indicating that **3** has the least anisotropy in the coordination planeThe comparatively low resolution could explain the exception to the trend identified above.

All three compounds exhibit rhombic bond geometry as seen in Table 2, where each coordination center in **1**-**3** is 6-coordinate distorted octahedral. This agrees with the rhombic electronic structure seen in the fits of the EPR data, with three distinct g-factor values. The Lorentzian contribution to the two-regime linewidth system is consistently larger than the Gaussian contribution for each compound. This indicates that the dipolar interactions are weaker than the exchange interactions, since the Gaussian regime is associated with dipolar interactions and the Lorentzian regime is associated with exchange-narrowed systems.[29]

Table 5. Difference between the corresponding values from results at X-band and Q-band (Table 4).

	Δg_x	Δg_y	Δg_z	GC	LC	RMSD
1	0.0052	0.0044	0.0078	0.0743	0.0396	-0.0061
2	0.0066	0.0051	0.0085	0.2111	0.0707	-0.0071
3	0.0054	0.0052	0.0088	0.0524	-0.8571	-0.0079

Magnetization Data

Magnetization as a function of applied field was collected for **1**-**3** (Figures 17, S5, S6) at 1.8 K between 0 - 50 kOe. All three data sets show slight upward curvature in agreement with a low-dimensional magnetic system.[30] None of the compounds near the expected saturation magnetization for an S = ½ system with g slightly greater than 2 (~6,000 emu/mol) in agreement with the presence of moderate antiferromagnetic exchange in the systems. At 50 kOe, the maxima are 1,170 emu/mol, 1,260 emu/mol and 1,010 emu/mol for **1**-**3** respectively. The significantly lower magnetization of **3** at 50 kOe suggests the presence of stronger interactions in the compound (an overlay of the three graphs is shown in Figure S7).

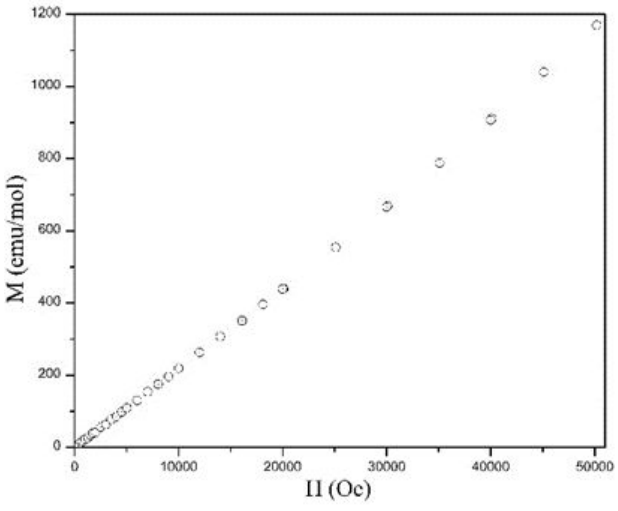

Figure 17. M(H) at 1.8 K for **1**.

Susceptibility data were collected from 1.8-310 K in an applied field of 1 kOe and are shown in Figures 18, S8 and S9 for **1**-**3** respectively. All three compounds exhibit a rounded maximum in the region 6-9

K indicating the presence of antiferromagnetic interactions in the samples. The data were fit to the models for an S = ½ Heisenberg chain both with and without a Curie-Weiss term to take interchain interactions into account.[30] The fitting results are presented in Table 6.

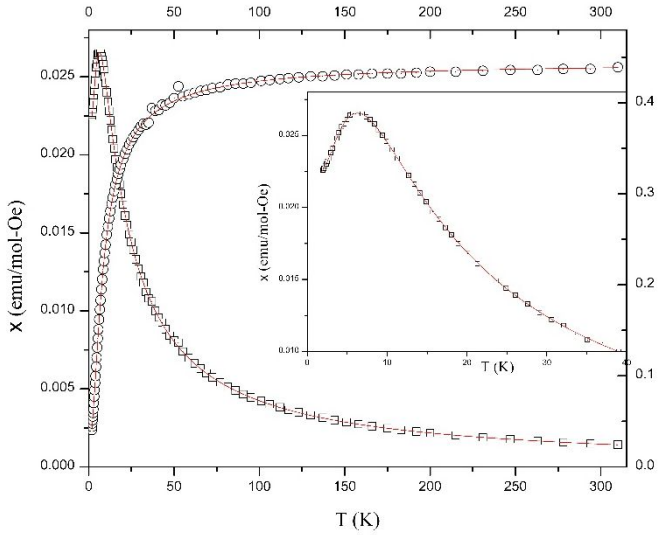

Figure 18. χ(T) (□) and χT(T) (○) for **1**. The solids lines represent the best fit to the S = ½ Heisenberg chain model with a Curie-Weiss correction to account for interchain interactions. The inset shows an expansion of the χ(T) data in the region of the maximum.

Table 6 - Fitted parameters for temperature dependence of susceptibility for **1**-**3**. C = Curie constant, J = exchange constant, θ = Weiss constant, p = paramagnetic impurity.

Model	C (emu-K/ mol-Oe)	J/k_B (K)	θ (K)	p (%)
1				
χ(T)	0.432(1)	-9.85(1)		0.35(1)
χ(T) - CW	0.432(1)	-9.89(1)	0.06(3)	0.1(f)*
χT(T)	0.431(1)	-9.77(2)		0.2(1)
χT(T) - CW	0.431(1)	-9.81(5)	0.04(3)	0.1(f)*
2				
χ(T)	0.446(1)	-9.186(7)		0.06(1)
χ(T) - CW	0.447(1)	-9.16(7)	-0.16(1)	0.7(4)
χT(T)	0.449(1)	-9.36(3)		0.41(17)
χT(T) - CW	0.449(1)	-9.18(8)	-0.14(4)	0.7 (1)
3				
χ(T)	0.444(1)	-11.00(1)		0.46(15)
χ(T) - CW	0.443(1)	-11.09(2)	0.14(4)	0.1(f)*
χT(T)	0.441(1)	-10.80(5)		0.77(1)
χT(T) - CW	0.441(1)	-10.96(7)	0.2(2)	0.2(2)

*In a few cases, the fitted paramagnetic impurity percentage was negative, but zero within the fitting error. Those values were fixed at 0.1%.

Good agreement is seen between the fitting results when comparing fits of χ(T) or χT(T), with parameters generally within the error, whether including a Curie-Weiss correction for interchain interactions or not. The Weiss constants are negligible in all cases, suggesting good isolation between the chains. Small, but significant differences are seen between the exchange constants with J_{ave} increasing in the order **2** < **1** < **3**. The absence of any discontinuity in the temperature dependent data for **2** indicates that any change in magnetic properties due to the crystallographic phase change is negligible.

Discussion

The complexes are all centrosymmetric, pyrazine-bridged coordination polymers. The staggering of adjacent chains with respect to the pyridone molecules and the separation between chains caused by the hydrogen bonding of the water molecules to the perchlorate ions prevent formation of any traditional magnetic superexchange pathways between those chains. The Cu(II) ions are pseudo-octahedral and exhibit classical Jahn-Teller elongations with the water molecules lying along the JT axis. Although the geometry at the Cu ions is fundamentally the same for all three compounds, there are some small differences observed. Considering only the low-temperature structures, the Cu-O_{water} bond lengths increase in the order **2** < **1** < **3** while the Cu1-N1 bond lengths increase in the order **3** < **1** **2** and the Cu-O12 bonds (to the pyridone ring) increase from **2** < **1** **3**. This is likely a steric effect as the methyl group in **2** is furthest away from the Cu-coordination sphere. The C12-O12 bond lengths (within the pyridone ring) are the same within error in all three structures suggesting that the position of the methyl group does not affect the degree of double bond character in a measurable way.

The changes in coordination and ligands result in differences in the EPR spectra. Although all three compounds are rhombic in nature, the degree of rhombicity (difference between g_x and g_y) is highly variable. At X-band, **1** and **2** appear to be rhombic with clear inflection points seen at higher field. Compound **3**, on the other hand, qualitatively appears to be axial with no visible inflection, in spite of the three clearly distinct axes from the crystal structure. Q-Band spectra cleanly resolve the g_x and g_y components of the spectra for **1** and **2**, and more importantly, show that **3** is also rhombic, albeit with a very small difference between g_x and g_y. This suggests an accidental near equivalence of the crystal field contributions from the pyrazine and pyridone ligands in **3**.

Susceptibility measurements are well fit by the uniform chain model and show very good isolation as demonstrated by negligible θ values and differences in parameters whether an interchain interaction term is included in the fitting or not. Curie constants for the three compounds are nearly the same as would be expect given the similarity of the compounds. In addition, the fitted values agree extremely well with the measured g-values for the compounds. Using the measured g-factors, one calculates C = 0.433, 0.435, and 0.432 emu-K/mol-Oe for **1**-**3** respectively, compared to fitted values of 0.432, 0.446 and 0.444 emu-K/mol-Oe for **1**-**3** (from the χT(T) fits). However, there is a small, but experimentally distinct, difference in the J-values with **2** slightly less than **1**, and **3** the largest by ~15%. These values correlate with two of the structural parameters. The length of the Cu-O_{water} bond is inversely proportional to the value of J. Lengthening of the bonds along the J-T axis would lead to greater separation of the d_{z^2} and $d_{x^2-y^2}$ orbitals and a greater localization of the unpaired electron density in the latter orbital, which is a contributor to the bonding along the

pyrazine-bridged superexchange pathway. The change in Cu-O12 bond lengths also supports this trend with longer Cu-O12 bonds allowing for greater overlap of the Cu-pyrazine orbitals.

Although there are few pyrazine-bridged Cu(II) chains reported with an N_2O_4 coordination sphere, four closely related compounds have been recently described. Two of the compounds are substituted 4-pyridone analogues of the current complexes, $[CuL_2(H_2O)_2(pz)](ClO_4)_2$ [L = 3-bromo- or 3-chloro-4-pyridone].[31] These compounds also exhibit 1D-Heisenberg type antiferromagnetic chain behavior with negligible interchain interactions. The fitted J/k_B values are 8.47(2) K (Cl) and 8.12(1) K (Br). A comparison of these J values and the corresponding Cu-O_{water} bond lengths shows the opposite trend, with the shorter bond (2.348(2) Å) corresponding to the chloro-substituted compound (larger J) and the longer bond (2.360(7) Å) corresponding to the bromo-substituted compounds (smaller J). Both compounds exhibit weaker exchange than **1**-**3**. The Cu-N bond lengths are identical within the error.

Two additional compounds follow the N_2O_6 coordination sphere motif, but in these the ancillary L is pyridine-N-oxide, $[Cu(pyridine\text{-}N\text{-}oxide)_2(H_2O)_2(pz)](An)_2$, where the anion (An) is either ClO_4[32] (as in the current work) or PF_6.[20d] In these complexes, the perchlorate salt shows the shorter Cu-O_{water} bond (by ~ 0.08 Å) but the Cu-Opy bond is slightly shorter (~0.02 Å) in the hexafluorophosphate salt. The perchlorate compound exhibits a slightly larger exchange constant of -9.6(1) K compared to the hexafluorophosphate compounds (-8.8(2) K). Here, however, the difference in exchange constants correlates with the difference in Cu-N bond lengths with the perchlorate shorter by ~ 0.01Å. This provides a range of exchange strengths which differ by 30% from the strongest to the weakest. However, the difference in ligand types makes direct comparison from one family to the next tenuous and supports the principle that there are a wide variety of factors contributing to the exchange. The need for more complexes within one closely-knit family is definite.

Conclusions

A family of pyrazine-bridged Cu(II) uniform chain compounds, differing by the position of the methyl substituent on the ancillary pyridone ligand, has been prepared and analyzed by single-crystal X-ray diffraction, EPR and variable temperature magnetic susceptibility measurements. The position of the methyl substituent results in significant changes in the crystal structures (three different space groups) and more subtle changes in the local structures. Compound **2** exhibits a crystallographic phase transition near 170 K, with a concomitant lowering of the crystallographic symmetry and a color change. EPR measurements show that all three compounds exhibit rhombic symmetry, as expected from the crystal structures, but in the case of **3**, the spectra are very nearly axial despite the apparent distinctions of the coordination axes. Magnetic susceptibility measurements show antiferromagnetic exchange in all three, with small changes in the value of J which correlate well with the degree of Jahn-Teller distortion at the Cu ion and with the Cu-N bond length, although the latter changes are quite small. Further experiments are in progress with a wide variety of electron donating and withdrawing substituents on the pyridone ring including halogen, cyano and nitro groups.

Conflicts of interest

There are no conflicts to declare.

Acknowledgements

Funding for the powder X-ray diffractometer and SQUID magnetometer was provided by a Kresge Foundation grant, PolyCarbon Industries Inc. (now SEQENS), and the National Science Foundation. EKD is grateful for support from an anonymous donor, the Frederick M. and Alice Murdock Research Fund and from Norwood Laboratories. FEW is grateful for support from PolyCarbon Industries (now SEQENS).

References:

1. a) O. Kahn, *J. Chim. Phys. Phys.-Chim. Biologique* 1988, **85**, 1113. b) K. Awaga, *Kotai Butsuri* 1995, **30**, 281. c) D. Gatteschi, *Advanced Materials* (Weinheim, Germany) 1994, **6**, 635. d) J. Villain, *Frontiers of Neutron Scattering*, Proceedings of the 7th Summer School on Neutron Scattering, (ed. A. Furrer), Zuoz, Switzerland, 2000, 131.

2. a) I. Castro, M.L. Calatayud, C. Yuste, M. Castellano, R. Ruiz-Garcia, J. Cano, J. Faus, M. Verdaguer and F. Lloret, *Polyhedron* 2019, **169**, 66. b) F.-S. Guo, A.K. Bar and R.A. Layfield, *Chem. Rev.* 2019, **119**, 8479. c) M. Andruh, *Chem. Commun.* 2018, 54, 3559. d) D. Maniaki, E. Pilichos and S.P. Perlepes *Front. in Chem.* 2018, **6**, 461.

3. a) J.C. Bonner, *NATO ASI Series, Series C:* Mathematical and Physical Sciences 1985, **140** (Magn.-Struct. Correl. Exch. Coupled. Syst.), 157. b) J.C. Bonner and M.E. Fisher, *Phys. Rev.* 1964, **135**, A640.

4. A.V. Santoro, A.D. Mighell and C.W. Reimann, *Acta Crystallogr. Sect. B*: 1970, **26**, 979.

5. a) Y. Kono, T. Sakakibara, C.P. Aoyama, C. Hotta, M.M. Turnbull, C.P. Landee and Y. Takano, *Phys. Rev. Lett.* 2015, **114**, 037202/1-5.

b) P.D.W. Boyd and S. Mitra, *Inorg. Chem.* 1980, **19**, 3547. c) D.B. Losee, H.W. Richardson and W.E. Hatfield, *J. Chem. Phys.* 1973, **59**, 3600. d) W.E. Hatfield and J.F. Villa, *J. Am. Chem. Soc.* 1971, **93**, 4081.

6. a) Y. Ishikawa, K. Ohya, Y. Fujii, Y. Koizumi, S. Miura, S. Mitsudo, A. Fukuda, T. Asano, T. Mizusaki, A. Matsubara, H. Kikuchi and H. Yamamori, *J. Infra. Millim. Terahz. Waves* 2018, **39**, 288. b) A.A. Validov, M. Ozerov, J. Wosnitza, S.A. Zvyagin, M.M. Turnbull, C.P. Landee and G.B. Teitel'baum, *J. Physics: Cond. Matt.* 2014, **26**, 026003/1-5. c) G.F. Kokoszka and C.W. Reimann, *J. Inorg. Nucl. Chem.* 1970, **32**, 3229.

7. B.R. Jones, P.A. Varughese, I. Olejniczak, J.M. Pigos, J.L. Musfeldt, C.P. Landee, M.M. Turnbull and G.L. Carr, *Chem. Materials*, 2001, **13**, 2127.

8. a) I.O. Thomas, S.J. Clark and T. Lancaster, *Phys. Rev. B* 2017, **96**, 094403/1-8. b) J. Jornet-Somoza, M. Deumal, M.A. Robb, C.P. Landee, M.M. Turnbull, R. Feyerherm and J.J. Novoa, *Inorg. Chem.* 2010, **49**, 1750.

9. a) H. Kuhne, A.A. Zvyagin, M. Gunther, A.P. Reyes, P.L. Kuhns, M.M. Turnbull, C.P. Landee and H.-H. Klauss, *Phys. Rev. B* 2011, **83**, 100407/1-4. b) H. Kuehne, H.-H. Klauss, S. Grossjohann, W. Brenig, F.J. Litterst, A.P. Reyes, P.L. Kuhns, M.M. Turnbull and C.P. Landee, *Phys. Rev. B.* 2009, **80**, 045110/1-5.

10. a) F. Xiao, J.S. Moller, T. Lancaster, R.C. Williams, F.L. Pratt, S.J. Blundell, D. Ceresoli, A.M. Barton and J.L. Manson, *Phys. Rev. B* 2015, **91**, 144417/1-8. b) S.J. Blundell, T. Lancaster, F.L. Pratt, P.J. Baker, M.L. Brooks, C. Baines, J.L. Manson and C.P. Landee, *J. Phys. Chem. Sol.* 2007, **68**, 2039. c) T. Lancaster, S.J. Blundell, M.L. Brooks, P.J. Baker, F.L. Pratt, J.L. Manson, C.P. Landee and C. Baines, *Phys. Rev. B* 2006, **73**, 020410/1-4.

11. M.B. Stone, D.H. Reich, C. Broholm, K. Lefmann, C. Rischel, C.P. Landee and M.M. Turnbull, *Phys. Rev. Lett.* 2003, **91**, 037205/1-4.

12. a) J. Rohrkamp, M.D. Phillips, M.M. Turnbull and T. Lorenz, *J. Phys.: Conf. Ser.* 2010, **200**, 012169/1-4. b) G. Mennenga, L.J. De Jongh, W.J. Huiskamp and J. Reedijk, *J. Magn. Magn. Mat.* 1984, **44**, 89.

13. L.H.R. Dos Santos, A. Lanza, A.M. Barton, J. Brambleby, W.J.A. Blackmore, P.A. Goddard, F. Xiao, R.C. Williams, T. Lancaster, F.L. Pratt, S.J. Blundell, J. Singleton, J.L. Manson and P. Macchi, *J. Am. Chem. Soc.* 2016, **138**, 2280.

14. O. Breunig, M. Garst, A. Klümper, J. Rohrkamp, M.M. Turnbull and T. Lorenz, *Science Advances* 2017, **3**, eeao3773.

15. a) J. Jornet-Somoza, N. Codina-Castillo, M. Deumal, F. Mota, J.J. Novoa, R.T. Butcher, M.M. Turnbull, B. Keith, C.P. Landee and J.L. Wikaira, *Inorg. Chem.* 2012, **51**, 6315. b) R.T. Butcher, L.N. Dawe, C.P. Landee and M.M. Turnbull, *Polyhedron* 2009, **28**, 1710. c) K.D. Hughey, N.C. Harms, K.R. O'Neal, A.J. Clune, J.C. Monroe, A.L. Blockmon, C.P. Landee, Z. Liu, M. Ozerov, J.L. Musfeldt, Inorg. Chem. 2020, 59, 2127.

16. F.M. Woodward, P.J. Gibson, G.B. Jameson, C.P. Landee, M.M. Turnbull and R.D. Willett, *Inorg. Chem.* 2007, **46**, 4256. b) J.L. Manson, J.A. Schlueter, K.A. Funk, H.I. Southerland, B. Twamley, T. Lancaster, S.J. Blundell, P.J. Baker, F.L. Pratt, J. Singleton, R.D. McDonald, P.A. Goddard, P. Sengupta, C.D. Batista, L. Ding, C. Lee, M.-H. Whangbo, I. Franke, S. Cox, C. Baines and D. Trial, *J. Am. Chem. Soc.* 2009, **131**, 6733. c) R. Scatena, F. Montisci, A. Lanza, N.P.M Casati, P. Macchi *Inorg. Chem*. 2020, **59,** 10091. d) S. Kwon, M. Jeong, M. Kubus, B. Wehinger, K.W. Kramer, Ch. Ruegg, H.M. Roennow, S. Lee *Phys. Rev. B* 2019, **99**, 214403.

17. a) R.T. Butcher, C.P. Landee, M.M. Turnbull and F. Xiao, *Inorg. Chim. Acta*. 2008, **361**, 3654. b) J. Pickardt and B. Staub, *Z. Naturforsch., B: Chem. Sci*. 1997, **52**, 1456. c) T. Fetzer, A. Lentz and T. Debaerdemaeker, *Z. Naturforsch., B: Chem. Sci.* 1989, **44**, 553.

18. C. Sen, M. Kumar, Z. ul Nisa, N. Akhter Ashashi, A. Frontera, S. Chandra Sahoo, H. Nawaz Sheikh, *Polyhedron* 2020, **187**, 114629.
19 a) P. Perlepe, I. Oyarzabala,K.S. Pedersen, P. Negrier, D. Mondieig, M. Rouzières, E.A. Hillard, F. Wilhelm, A. Rogalev, E.A. Suturina, C. Mathonière, R. Clérac *Polyhedron* 2018, **153**, 248. b) K.S. Pedersen, P. Perlepe, M.L. Aubrey, D.N. Woodruff, S.E. Reyes-Lillo, A. Reinholdt, L. Voigt, Z. Li, K. Borup, M. Rouzières, D. Samohvalov, F. Wilhelm, A. Rogalev, J.B. Neaton, J.R. Long, R. Clérac *Nature Chem*. 2018, **10**, 1056. c) H. Xie, Q. Yu, I. Muhammad, Q. Sun*, J. Physics: Cond. Matt.* 2020, **32**, 135801. d) J. Palion-Gazda, K. Choroba, B. Machura, A. Switlicka, R. Kruszynski, J. Cano, F. Lloret, M. Julve, *Dalton Trans*. 2019, **48**, 17266.

20. a) A. Majumder, V. Gramlich, G.M. Rosai, S.R. Batten, J.D.

Masuda, M.S.E. Fallah, J. Ribas, J.-P. Sutter, C. Desplanches and S. Mitra, *Cryst. Growth Des.* 2006, **6**, 2355. b) J.L. Manson, M.M. Conner, J.A. Schlueter and K.A. Hyzer, *Polyhedron* 2007 **26**, 1912. c) P.A. Goddard, J. Singleton, P. Sengupta, R.D. McDonald, T. Lancaster, S.J. Blundell, F.L. Pratt, S. Cox, N. Harrison, J.L. Manson, H.I. Southerland and J.A. Schlueter, *New J. Phys.* 2008, **10**, 083025. d) P.A. Goddard, J.L. Manson, J. Singleton, I. Franke, T. Lancaster, A.J. Steele, S.J. Blundell, C. Baines, F.L. Pratt, R.D. McDonald, O.E. Ayala-Valenzuela, J.F. Corbey, H.I. Southerland, P. Sengupta and J.A. Schlueter, *Phys. Rev. Lett.* 2012, 108, 077208. e) J. Darriet, M.S. Haddad, E.N. Duesler and D.N. Hendrickson, *Inorg. Chem*. 1979, **18**, 2679.

21. J. Liu, P.A. Goddard, J. Singleton, J. Brambleby, F. Foronda and J.S. Moller, *Inorg. Chem*. 2009, **55**, 3515.

22. J.X. Yuan, M.L. Hu, Y.Q. Cheng, L.C. Chen and S.W. Ng, *Acta Cryst. C* 2002, **58**, M270-272.

23. G. M. Sheldrick, *Acta Crystallogr. A*, 2008, **64,** 112.

24. G.M. Sheldrick, *Acta Crystallogr. A*, 2015, **71**, 3 (2015).

25. G.M. Sheldrick, *Acta Crystallogr. C*, 2015 **71**, 3.

26. R. L. Carlin. Magnetochemistry, *Springer-Verlag* (1986) Berlin.

27. S. Stoll and A Schweiger, *J. Magn. Reson.* 2006, **178(1)**, 42.

28. MATLAB. 2010, *The MathWorks Inc.* Version 9.4.0 (R2018a).

29. A. Bencini and D. Gatteschi, *Dover Publications, Inc.* New York, 2012, 482.

30. C.P. Landee and M.M. Turnbull, *J. Coord. Chem.,* 2014, **67**, 375-439.

31. J.C. Monroe, C.P. Landee, M.M. Turnbull, J.L. Wikaira, *J. Coord. Chem.* in press.

32. C.P. Landee, E. Kirkman-Davis, M.M. Turnbull, M. Polson, J.L. Wikaira, submitted for publication in *J. Coord. Chem*.

Graphical Table of Contents Entry

The reaction of pyrazine copper (II) perchlorate and n-methyl-2(1H)-pyridone (L) generates a family of uniform S = ½, antiferromagnetic chains $[CuL_2(H_2O)_2pz](ClO_4)_2$. The compounds were studied crystallographically and by EPR and magnetic susceptibility measurements. The strength of the magnetic exchange correlates with the elongation of the Cu-O_{water} bond along the Jahn-Teller axis.